International Journal of Thermal Sciences 50 (2011) 1001–1012

Contents lists available at ScienceDirect

International Journal of Thermal Sciences

journal homepage: www.elsevier.com/locate/ijts

Axial conduction in single-phase simultaneously developing flow in a rectangular mini-channel array

Manoj Kumar Moharana, Gaurav Agarwal, Sameer Khandekar*

Department of Mechanical Engineering, Indian Institute of Technology Kanpur, Kanpur (UP) 208016, India

ARTICLE INFO

Article history:
Received 13 January 2010
Received in revised form
17 January 2011
Accepted 18 January 2011
Available online 22 February 2011

Keywords:
Mini–microchannels
Simultaneously developing flow
Heat and momentum flux transfer
Axial conduction
Conjugate effects

ABSTRACT

Thermo-hydrodynamic performance of hydrodynamically and thermally (simultaneously) developing single-phase flow in an array of rectangular mini-channels has been experimentally and numerically investigated. The test section consists of fifteen rectangular parallel mini-channels of width 1.1 ± 0.02 mm, depth 0.772 ± 0.005 mm (aspect ratio $= 0.7$, hydraulic diameter $= 0.907$ mm), inter-channel pitch of 3.1 mm, machined on a copper substrate of thickness 8.0 mm and having an overall length of 50 mm. Deionized water used as the working fluid, flows horizontally and the test section is heated by a thin surface-mountable, stripe heater (constant heat flux boundary condition applied at the bottom of the substrate; top face being adiabatic). Reynolds number (Re) between 150 and 2500 and Prandtl number between 3 and 4, at an inlet pressure of about 1.1 bar, are examined. The laminar-to-turbulent transition is found to commence at Re $\approx$ 1100 for average channel roughness of 3.3 μm ($\varepsilon/D_h = 0.364\%$). Poiseuille (Po) and local Nusselt number (Nu_x) are function of flow Re in the entire range of experiments. Experimental data for Po and Nu_x are compared with available correlations for simultaneously developing flows in rectangular channels. A 3D numerical CFD model, exactly corresponding to the geometry and boundary conditions of the experimental setup, has also been developed. Conservation equations have been solved in the conjugate domain to explore conjugate heat transfer effects leading to deviation from true constant heat flux conditions. It is observed that at higher value of the axial conduction number (M), the experimental setup is prone to conjugate effects as a consequence of axial back conduction in the substrate. Due to this, local experimental Nusselt numbers are not only smaller than the actual counterparts predicted by the model, but also their axial variation is affected. Apart from the fact that transition occurs early, no new physical phenomena or effects are observed in the data. Most parallel channels connected to a common inlet header will have fully or partially developing flows. In addition, depending on the geometry and flow conditions (i.e. parameter M), conjugate heat transfer effects become predominant; therefore, the data should be carefully interpreted in this context and background.

1. Introduction

In recent years, there is a rapid growth of applications which require high heat transfer rates and fluid flows in relatively small passages. Some examples, which demand such flow conditions, are electronics cooling, space thermal management, MEMS devices for biological and chemical reactors, etc. The development of new applications requiring cooling of components in a confined space has motivated researchers to focus on the prediction of the thermo-hydrodynamic performance of mini and microchannels.

Though the words *minichannel* and *microchannel* appear frequently in the literature, there is no generally accepted demarcation of their regimes. The hydraulic diameter ($D_h = 4A/\zeta$) of the channel array used in this experimental study is 0.907 mm. Looking into the recent literature, this will be categorized as a 'mini-channel' [1], although alternate available definitions may also classify this hydraulic diameter as a 'microchannel' [2]. Despite the fundamental simplicity of laminar flow in straight ducts, experimental studies of mini/microscale flow have often failed to reveal the expected relationship between the transport parameters (e.g., friction factor and Reynolds number, flow transition limits). Furthermore, data for simultaneously developing flows, which inherently provide high species transport coefficients and therefore of practical interest, are not very abundant. Specific correlations for simultaneously developing flows for non-circular channels for the entire range of Pr and geometrical parameters, have also limited availability. In this context, before proceeding to describe the nuances of the present study, the relevant literature is reviewed in the next section.

* Corresponding author: Tel.: +91 512 259 7038; fax: +91 512 259 7408.
E-mail address: samkhan@iitk.ac.in (S. Khandekar).

1290-0729/$ – see front matter © 2011 Elsevier Masson SAS. All rights reserved.
doi:10.1016/j.ijthermalsci.2011.01.017

Nomenclature

A	area of cross-section (m^2)
c_p	specific heat at constant pressure (J/kg K)
D	diameter (m)
f	Darcy friction factor (−)
h	heat transfer coefficient (W/m^2 K)
$K(\infty)$	incremental pressure-drop number for fully-developed flow (−)
k	thermal conductivity (W/m K)
L	length of the channel, characteristic length (m)
M	axial heat conduction number (−)
NTU	number of transfer units (−)
P	pressure (N/m^2)
p	channel pitch (m)
Q	heat power (W)
$\dot{q}''$	heat flux (W/m^2)
T	temperature (K)
T^*	non-dimensional temperature (−)
u	velocity (m/s)
w	width of channel (m)
X	entry length (m)
x	distance from inlet (m)
x_+	non-dimensional distance ($=x/\mathrm{Re}D_h$)
x^+	non-dimensional distance ($=x/\mathrm{RePr}D_h$)

Greek symbols

α	depth/width (aspect) ratio of rectangular channels (−)
δ	thickness (m)
ε	surface roughness parameter (m)
μ	dynamic viscosity (Pa s)
ρ	mass density (kg/m^3)
ζ	wetted perimeter (m)
ξ	length ratio (−)

Non-dimensional numbers

Bi	Biot number (hL_c/k_w)
Nu	Nusselt Number (hL_c/k_f)
Po	Poiseuille Number (fRe)
Pr	Prandtl Number ($c_p\mu_f/k_f$)
Re	Reynolds Number ($\rho uL_c/\mu_f$)

Subscripts

app	apparent
c	characteristics
cf	constricted flow
cond	conductive
conv	convective
cr	critical
f	fluid
fd	fully developed
h	hydraulic, hydrodynamic
i	inlet
m	mean
o	outlet
th	thermal
w	wall
x	local value

2. Literature review

During the last two decades, the focus has shifted from macro size channels/pipes to their mini/micro counterparts, mainly in search of efficient cooling of high heat flux dissipating devices. The potential of micro channel arrays for high heat flux removal from electronics chips was first demonstrated in 1981 by Tuckerman and Pease [3]. This novel idea led to a number of innovative designs and spawned extensive research efforts in the area of micro-channel cooling. Following this study, Wu and Little [4] conducted experiments to measure flow friction along with heat transfer characteristics of gases (N_2, H_2, Ar) flowing in silicon/glass microchannels having trapezoidal cross-section ($D_h = 55.81$, 55.92 and 72.38 μm). Experimental friction factors were found to be larger (10–30%) than those predicted by the conventional theory. They concluded that the deviations were due to the large ε/D_h and its asymmetric distribution on the channel walls. Subsequent to these studies, considerable interest was generated in augmenting transport coefficients through mini/microchannels. Most works have been directed at quantifying the effects of flow parameters and channel dimensions on the local and bulk transport characteristics, numerical modeling and experimentation to find new scaling laws, flow geometry optimization and scrutiny of special microscale effects. Comprehensive review articles concerning heat transfer and pressure drop of single-phase flow in mini/microchannels have been presented from time to time by several authors [5–13]. In the following section, selected recent literature relevant to the present study is highlighted.

Lee and Garimella [14] investigated laminar convective heat transfer in the entrance region of rectangular cross-section microchannels subjected to H1 boundary condition (H1: axially uniform wall heat flux and circumferentially uniform wall temperature). Based on numerical simulations they proposed correlations to predict local and average Nusselt number (for inlet Pr = 5.83). They found that their proposed correlations are in very good agreement with available experimental data. Earlier Lee et al. [15] conducted a detailed three dimensional conjugate heat transfer analysis for a copper microchannel heat sink subjected to uniform heat flux imposed on the bottom of the substrate. They compared the results from their analysis to those obtained from simplified analyses for a microchannel using the H1, H2 and T boundary conditions on the channel wall (H2: uniform wall heat flux, both axially and circumferentially; T: uniform wall temperature, both axially and circumferentially). They concluded that the H1 thermal boundary condition is the most appropriate for simplified analyses, when full conjugate analyses are not computationally affordable as the H1 thermal boundary condition is common in engineering problems with highly conductive wall materials.

Bahrami et al. [16] studied pressure drop of fully-developed laminar flow in smooth arbitrary cross-sections channels to find relationship for $f\mathrm{Re}_{\sqrt{A}}$ using existing analytical solutions. They found that square root of cross-sectional area $\sqrt{A}$, as the length scale, is superior to the conventional hydraulic diameter D_h. Earlier, Muzychka and Yovanovich [17] had showed that the apparent friction factor is a weak function of the geometrical shape of the channel (aspect ratio). Based on these recommendations, Bahrami et al. [16] proposed a compact approximate model as a function of cross-section geometry parameters (i.e. area, perimeter, and polar moment of inertia), that could predict pressure drop in a wide variety of channel shapes. They validated this model for rectangular, trapezoidal, square and circular cross-sections by comparing with experimental data and exact analytical solutions.

Celata et al. [18] experimentally investigated single-phase laminar flow in circular micro-ducts of diameter 528, 325, 259 and 120 μm. Results showed a decrease of Nusselt number with decreasing diameter, an axial dependence that is linked to thermal

entrance effects and a dependence of the Nusselt number also on Reynolds number. They also investigated the possible occurrence of scaling effects such as axial conduction in the walls, viscous heating of the fluid and thermal entrance length effects.

Steinke et al. [19] developed an experimental facility to study single-phase thermo-hydrodynamics of silicon microchannels. Flow rates were varied from 1 to 4000 ml/min, with heating input up to 1.5 kW. They found that diabatic friction factors are in agreement with conventional laminar Poiseuille flow theory after accounting for the entrance and exit losses and effects due to the developing region.

Zhigang et al. [20] experimentally studied heat transfer in quartz glass micro-tubes ($D = 45$, 92 and 141 μm, working fluid: deionized water) heated directly by a resistor coiled evenly around them. The results showed that the experimental Nusselt numbers obtained were less than the predictions of the classical laminar correlations at lower Reynolds number. This was explained due to the variation of the thermophysical properties with temperature and nonlinear temperature variation of the working fluid along the wall. With the increase of the Reynolds number ($Re > 1000$), the experimental Nu data were higher than the predictions by the classical transitional correlations. This was due to the conjugate effects of the thinner conductive liquid layer, the entrance length, the viscous dissipation and the wall roughness.

Yang and Lin [21] experimentally investigated heat transfer performance of water flowing through micro-tubes ($D = 123$–962 μm) using non-intrusive liquid crystal thermography. This investigation concluded that transition occurs at Re values 2300–3000. Conventional theory held good for fully-developed laminar and turbulent flow and heat transfer performance. Also, no significant size effect was observed for the range of diameters used. It was noted that the discrepancy in the Nusselt number for developing flows was found to increase with decreasing diameter.

Park and Punch [22] experimentally investigated friction factor and heat transfer of laminar flow ($69 < Re < 800$) through rectangular microchannels ($D_h = 106$–307 μm). It was found that, while conventional hydrodynamic theory for fully-developed flow is applicable for this range of flow Re, deviations were observed in heat transfer predictions. Therefore, they proposed an empirical correlation for Nu in terms of Re and Pr, the validity of which was limited to their experimental results. The authors also discuss the importance of geometrical design of the inlet manifold for achieving proper flow distribution in the parallel channel array.

García-Hernando et al. [23] experimentally studied the single-phase thermo-hydrodynamic performance of two microchannels of square cross-sections (100 and 200 μm respectively) using deionized water. They found that the experimental results, both for pressure drop and heat transfer, for a wide range of Reynolds numbers (except for very low Re), are in good agreement with the conventional theory; no special effects related to the small dimension of the channels were observed.

Natarajan and Christensen [24] studied effect of surface roughness on laminar, transitional, and turbulent regimes for fluid flow in microchannels using pressure-drop measurements and instantaneous velocity fields acquired by microscopic particle-image velocimetry. The experiment consisted of comparison of results from fluid flow through a smooth walled micro-channel of 0.45 μm width, 0.9 μm height, and two more channels (dimensions same as previous one) with vertical walls having RMS roughness value of $0.0125D_h$ and $0.025D_h$. The pressure-drop results of the smooth walled channel indicated onset of flow transition at $Re_{cr} > 1800$ along with deviation from laminar behavior at progressively lower Re with increasing roughness. Mean velocity profiles computed from the micro Particle-Image Velocimetry (μ-PIV) ensembles at various Re for each surface condition confirmed these trends, meaning Re_{cr} is a strong function of roughness.

Liu et al. [25] experimentally studied the influence of microscale effects on liquid flow resistance, viscous dissipation, wall roughness, etc. by using sensitive infra-red imaging (deionized water in micro-tubes with inner diameters of 19.6 and 44.2 μm). They found that experimental data closely matched the Hagen–Poiseuille predictions at lower Re values, and departs from classical theory at higher Re, attributed to the microscale effects.

In summary, experimental investigations on single-phase flow in mini/microchannels have focused mainly on the following aspects: (a) Flow transitions and critical Reynolds numbers, (b) Effect of channel shape, size and wall roughness on flow and heat transfer, and (c) Development of correlations for Po and Nu based on experimental measurements for various flow regimes, in terms of channel geometry and fluid properties (d) Effect of axial conduction, conjugate effects and critical scrutiny of the exactness of boundary conditions, etc. These studies reveal contradictory conclusions on many occasions and there are still important discrepancies between the results obtained by different researchers. This can be largely attributed to experimental uncertainties, effect of wall roughness, manifold design, control of boundary conditions in the experiment and conjugate effects. Secondly, limited combined fluid flow and heat transfer studies are available for simultaneously developing flows in mini–microchannels. Subtle differences are frequently present in the hardware design of mini–micro systems and the way in which 'mathematical' boundary conditions are experimentally achieved also differs in many works. So, there is a need of systematic data analysis and its careful scrutiny for simultaneously developing flows; this has very limited availability [26]. Correlations for simultaneously developing flows are also not readily available. Kandlikar et al. [13] have also highlighted the need for generating rigorous experimental data in this field. Most flows which take place through parallel channel arrays lead to fully or partially developing flows. Such flow arrangements are quite desirable in engineering applications for improved efficiencies. In this context, fluid flow and heat transfer characteristics of simultaneously developing flow in a copper mini-channel array ($D_h = 0.907$ mm, width (w) = 1.1 mm, depth (δ_f) = 0.772 mm and pitch (p) = 3.1 mm), subjected to constant heat flux at the bottom of the substrate, has been investigated in this work. Both experimental and numerical study on identical array geometry has been performed and the data are scrutinized for the effects of conjugate heat transfer on transport behavior.

3. Experimental details and procedure

The experimental facility was designed and constructed, as illustrated schematically in Fig. 1a. The test section consisted of an array of fifteen rectangular parallel mini-channels ($w = 1.1 \pm 0.02$ mm, $\delta_f = 0.772 \pm 0.005$ mm; $D_h = 0.907$ mm at $p = 3.1$ mm), machined on a copper substrate of 8 mm × 92 mm × 132 mm with each channel length = 50 ± 0.01 mm. The channel array was connected to inlet and outlet headers, both of size 50 mm × 20 mm × 0.8 mm respectively. Fig. 1b shows the actual photograph of the mini-channel test section. The grooved channels were covered by transparent polycarbonate sheet (8.0 mm thick) enabling flow visualization (flow boiling experiments were also done on the same test section, but not reported here) and providing necessary insulation from top of the test section. Fig. 1c shows the details of the array cross-section along the transverse and longitudinal planes respectively.

The uncertainty in determination of channel dimensions may lead to gross errors in the estimation of transport properties.

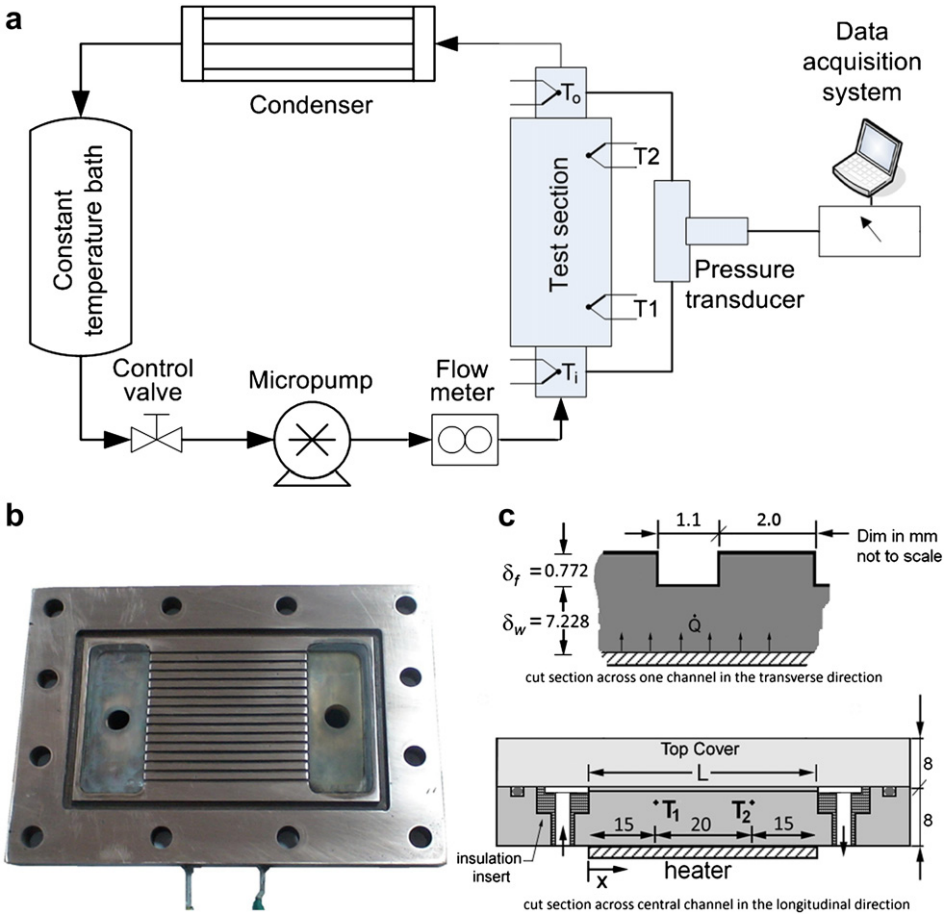

Fig. 1. (a) Schematic layout of the experimental setup showing the entire flow loop. (b) Photograph of upper surface (top view) of the mini-channel array. (c) Details of the mini-channel array showing the heater, thermocouples and insulation arrangement.

Therefore, the depth of the channel was measured with a high precision linear encoder (FAGOR® M-Series with resolution ±5 μm, accuracy ±10 μm). An optical microscope (Make: Leica® DM2500 M) was used to determine the channel width. Channel roughness parameters were measured at eight different locations along a channel using Laser Surface Profilometer (LSP Make: Mahr; vertical resolution 1 nm, horizontal resolution 0.1 μm) and then averaged to estimate the effective roughness. The effective value of average surface roughness for the entire array was found to be 3.3 μm ($\varepsilon/D_h = 0.364\%$) with standard deviation of 0.56 μm.

An electrically heated mica insulated strip-heater (50 mm × 50 mm × 1 mm, Make: Minco, HM6815R23.2) was attached below the copper substrate, using thermal contact heat sink compound (metal oxide filled silicon oil paste supplied by RS components®, thermal conductivity 2.9 W/m K), to heat the incoming working fluid, providing constant heat flux conditions at the bottom of the substrate; as noted above, the upper surface of the array was insulated (refer Fig. 1c). A digitally controlled DC supply (μTec®, PS8305D2) controlled the power to the strip-heater; a digital multimeter (accuracy ±0.1 V and ±0.01 A) measured the voltage and current across the heater.

The working fluid (distilled, degassed and deionized water) at a fixed temperature (maintained by a constant temperature bath, Haake® DC30K20, accuracy ±0.1 K) was allowed to pass through the mini-channel array via the inlet header. The fluid temperature at inlet and outlet of the test section was measured using two J-type thermocouples (Omega®, 0.5 mm bead diameter, accuracy ±0.1 after calibration) suitably located in the inlet and outlet headers. To calculate the wall temperature, two more J-type thermocouples were attached centrally along the channel length, at 15 mm from the both ends respectively and at a distance of 2.5 mm below the central channel wall, as shown in Fig. 1c. The Prandtl number of the fluid, as reported here, is based on the fluid temperature at the array inlet. To prevent the fluid from getting heated up in the inlet and outlet manifold, a plexiglass insulation insert ($k = 0.16$ W/m K) was attached to the substrate as shown in Fig. 1b and c.

The pressure drop across the test section was measured using a differential pressure transducer (Honeywell®: FP2000, Range 0–35,000 Pa, accuracy 0.1% of full scale reading; NIST traceable calibration). The tapping for the pressure transducer was made in the inlet and the outlet headers. Data acquisition was carried out using a high precision 16 bit DAQ (National Instruments®, PCI4351 with TBX-68T connector block) at 1 Hz and was designed on Lab-View® platform. Insulation (Glass wool fiber blanket covered with polystyrene foam sheet, thermal conductivity 0.036 W/m K at room temperature) was provided from all sides of the test section assembly and the assembly was integrated into a wooden box. The composite thickness of the insulation was about 35 mm on all the sides of the test section. Heat losses to the environment were estimated based on the conservation of energy; the difference between the electrical energy supplied to the channel and that received by the working fluid after steady state operation; loses were always less than ~8–11%.

4. Numerical modeling

Before proceeding to discuss the experimental results for pressure-drop and the heat transfer estimations obtained in the test section, it is important to answer two pertinent questions with respect to the present study. These questions are also relevant for many upcoming industrial heat transfer systems incorporating mini/microchannels.

(i) Is the flow distribution uniform across all the channels? Unless additional instrumentation is done in each mini-channel (which, most likely, may interfere with the flow) or a non-intrusive flow measurement technique is adopted (like μ-PIV), under usual conditions, it is not straightforward to experimentally answer this question. One of the most critical elements to achieve uniform flow distribution is the inlet manifold design [22].

(ii) Is the boundary condition at the channel wall close to constant heat flux, given the fact that the actual location of application of heat is at a certain finite distance from the channels? It is clear that the actual convective heat flux taken by the working fluid, substrate material properties, and its appropriate length scale, will affect the conductive heat transfer in the solid substrate domain; this will therefore influence the exactness of the boundary condition experienced by the working fluid at the channel wall. The constant heat flux boundary condition applied at a distance away from the channel wall may tend to be manifested as a "pseudo-constant-temperature" boundary condition to the incoming fluid, if there is sufficient back conduction or conjugate heat transfer effects in the substrate/array block, thereby affecting the experimentally estimated local and mean wall Nusselt number. Whether this phenomenon is occurring in the present test section and how is it related to the flow Reynolds number is also not 'directly' answerable with the present experimental instrumentation, although it can be inferred from the wall temperatures obtained at locations T1 and T2.

In real-time engineering applications too, fabrication of such heat transfer structures pose these two questions; if satisfactory reconciliation is not done it may lead to erroneous conclusions. Park and Punch [22] have discussed a suitable approach to address the first question of uniform flow distribution and highlight the importance of well designed inlet manifold. The issue of true boundary condition experienced by the fluid is also especially important in microscale geometries, as has been highlighted in recent literature [26–29].

To answer the above two questions in the context of the present experimental study and to validate the experimental results, a 3D computational fluid flow and heat transfer analysis of the experimental test section has also been undertaken. As noted above, it was not possible to answer both the posed questions by the present instrumentation and experimental technique. The CFD simulations were carried out using FLUENT®, commercially available software, under laminar flow conditions. The 3D model and the grid representing the exact dimensions of the experimental setup (one half of the experimental setup was modeled applying the available plane of symmetry to save computational efforts) was done using GAMBIT®. The schematic of the conjugate computational domain is as shown in Fig. 2. The entire solid and liquid domains were meshed using tetrahedrons consisting of over five million elements, about 2.2 million in the liquid domain and 2.8 million in the solid domain. The spatial grid resolution in longitudinal direction was 10^{-4} m (both solid and liquid) while in the transverse directions it was 10^{-6} m (in the liquid domain) and 10^{-5} m (in the solid domain). The 'Standard' scheme, available in FLUENT®, was used for pressure discretization. The SIMPLE algorithm was employed for pressure–velocity coupling. The conservation equation of mass, momentum and energy was solved using the second-order upwind scheme. Absolute convergence criterion set for momentum was 10^{-6} and for energy was 10^{-8}. Constant heat flux boundary condition was applied at the bottom of the substrate, exactly as in the experimental setup.

5. Results and discussion

In this section the experimental estimations of pressure-drop and heat transfer coefficient are discussed. Simultaneously, with the help of the numerical model, as described in Section 4, we also

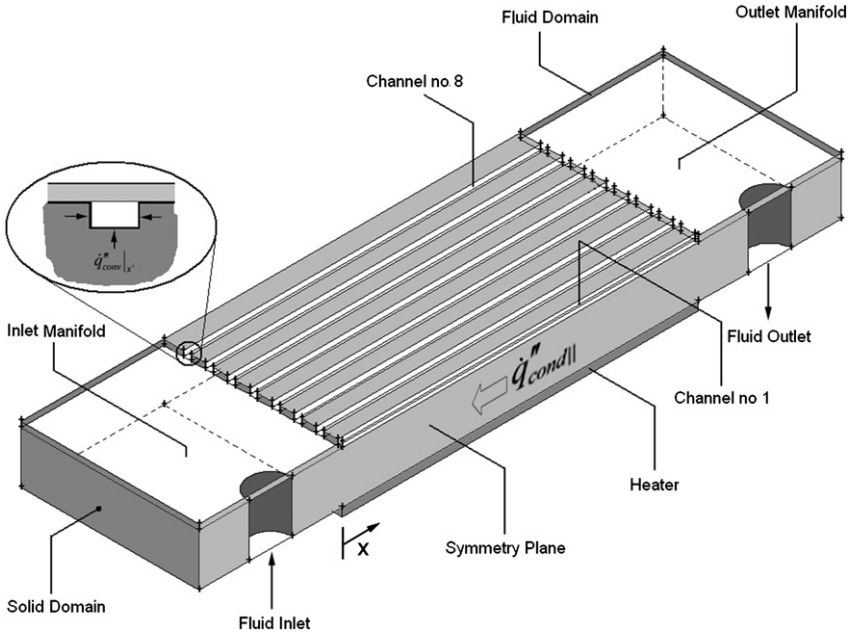

Fig. 2. Solid model (one-half portion) of the experimental test section.

scrutinize (a) the exactness of flow distribution in the test array and, (b) the actual boundary conditions at the channel wall experienced by the fluid. The predictions of transport coefficients under simultaneously developing flow conditions with the numerical model and available correlations respectively, and their comparison with the experimental data are also presented.

5.1. Pressure drop

Fig. 3 shows the flow distribution in the parallel channels, as obtained from the simulation. Channel number 1 denotes the central channel through which the symmetric plane passes (refer Fig. 2). The horizontal lines represent the corresponding mean flow rate through the respective channel estimated from the average pressure-drop calculation. It is found that for a given mean flow Re, although the flow rate through the central channel is somewhat higher than the rest of the channels (decreasing flow rate going from central channel 1 to channel 8), the deviation from mean flow rate for any channel is not more than 3.4% for the highest flow rates used in the experimental study. The inlet manifold, the way it is designed, essentially acts as an excellent reservoir plenum, maintaining near constant pressure conditions, which eventually leads to near uniform flow distribution in all the channels.

Based on the above results, all subsequent data reduction and estimations of transport coefficients were done on the basis of average constant mass flow rate in each channel.

The test section dimensions and experimental parameters were chosen in such a manner that the flow in the channels was always developing (both hydrodynamically and thermally) either along the full length of the channel or at least for some length of the channel from the inlet. Fig. 4 shows the hydrodynamic and thermal entry length estimations with respect to the flow Re, based on frequently used standard equations [30,31], which are noted on the figure.[1] As per these estimates, at Re ≈ 1100, the hydrodynamic entry length in laminar flow region is 49.89 mm, which is approximately equal to total channel array length, i.e. 50 mm. If the laminar-to-turbulent flow transition is believed to take place at Re = 2300 (conventional limit), then for all Re > 1100, the flow along the entire length of channel will be hydrodynamically developing in nature. For Re < 1100, the flow will fully develop somewhere inside the channel, as highlighted in Fig. 4. Experimental observations and comparison with simulation data (as described later in this section) indicate that the slope of the Po vs Re shows definite change at Re ≈ 900–1100, suggesting the inception of transitional flows, i.e. a drift away from laminarity. Considering that the flow is indeed in transition to turbulence at Re ≈ 1100, conventionally accepted first-order estimates suggest that the hydrodynamic entry length will then vary between $10D_h$ and $60D_h$. If the upper limit of $X_h = 60D_h$ is considered valid, then flow along the entire length of channel will remain hydrodynamically developing in nature for all Re > 1100. It should be noted, however, that Fig. 4 can, at best, be treated as a rough guideline; in practical reality the boundaries between developing and fully developed may be somewhat fuzzy due to intrinsic flow perturbations and inherent system/hardware design limitations [26].

As regards the thermal boundary layer development, since the applicable Prandtl number is in the range of Pr ≈ 3–4, under laminar flow conditions, flow is thermally developing along the entire channel length (refer Fig. 4; unless for Re < 350, in which case the flow will be thermally developing for some length of the channel only). For the case of turbulent flow, there is a possibility

[1] Although many definitions of hydrodynamic and thermal entry lengths are available, the one followed in this paper is as given by Shah and London [31].

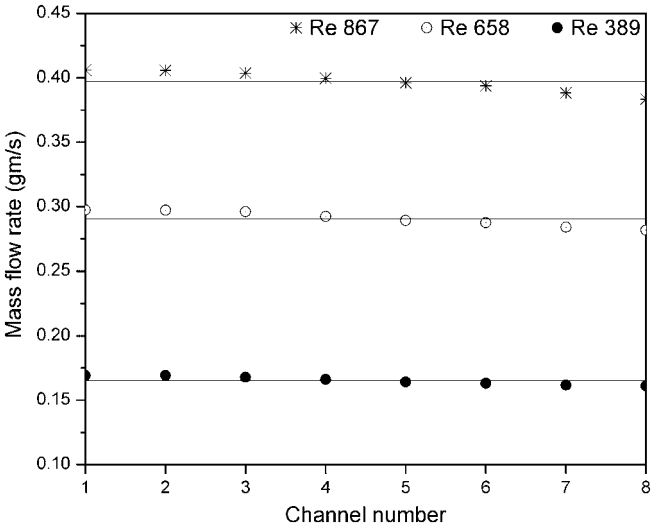

Fig. 3. Flow distribution across the parallel channels.

that flow thermally fully develops within the channel length, as suggested. Typically, a channel length greater than ten times hydraulic diameter is considered sufficient for full hydrodynamic and thermally turbulent flow development.

As the flow is developing in nature, the total pressure drop is due to friction as well as the change in the momentum flux in the hydrodynamic development length. For a constant density fluid, the net average pressure drop between duct lengths 0 to x, is correlated as

$$\left(\frac{\Delta P}{\frac{1}{2}\rho u^2 x_+}\right) = \left(4f_{\text{app}}\right)\cdot \text{Re} = \text{Po} \tag{1}$$

where, f_{app} is the apparent Fanning friction factor based on the total pressure drop in the channel; $x_+ = x/\text{Re}\cdot D_h$ is the dimensionless axial distance in the flow direction.

Fig. 5 (inset) shows the observed pressure drop in the array as a function of flow Re. The change of slope as well as some scatter in the raw data around Re ≈ 900–1100 is repeatedly observed in all experiments. As noted earlier in Fig. 4, the Reynolds number limit for the flow to remain completely developing inside the entire

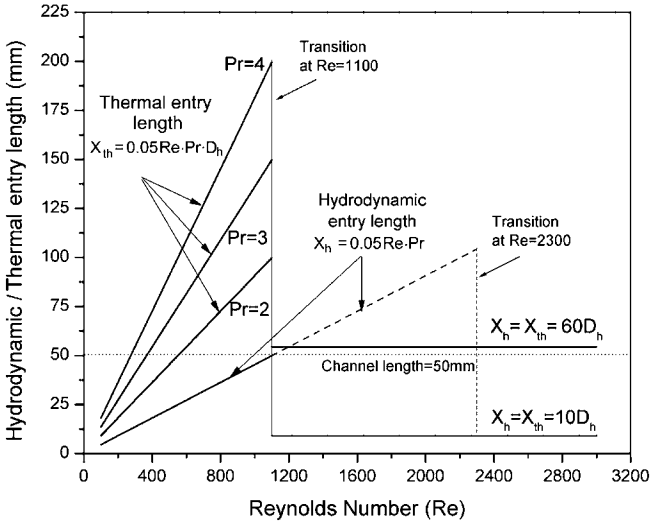

Fig. 4. Variation of hydrodynamic and thermal entry length with flow Re.

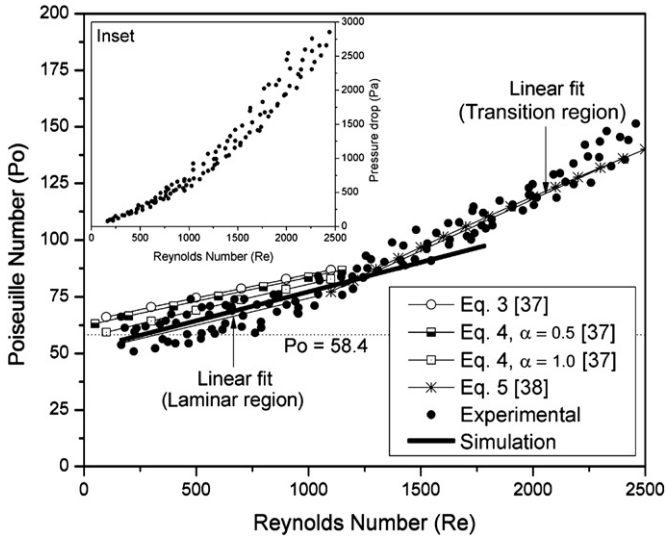

Fig. 5. Po vs Re for the entire experimental data set and its comparison with available correlations and the numerical model; inset shows the raw data, pressure drop vs flow Re.

channel length is Re = 1100. Thus, the data suggests that the flow is simultaneously getting affected by the inception of laminar-to-turbulent flow transition, which is indeed also a function of the development status of the velocity boundary layer in the channel. Such flow situations often come in compact high heat flux removal and electronics cooling applications. At this stage, it is difficult to clearly differentiate between these two effects (which, in fact, are strongly interrelated) and assign explicitly discernable explanation to the change of slope at Re ≈ 900–1100. It is to be noted that the transition from laminar-to-turbulent flow has been reported to occur in mini-channels at Re considerably below 2300 (e.g., Wu and Little [4], Natarajan and Christensen [24], Wang and Peng [32], Steinke and Kandlikar [33], etc.). Kandlikar et al. [34] have conducted experiments with stainless steel tubes with fully-developed flows and have also observed an early transition occurrence for ε/D_h of 0.355%. They have also suggested correlations for predicting transitions as a function of tube roughness for fully-developed flow conditions and re-plotted the classical Moody's Diagram with constricted flow diameter, defined as $D_{cf} = D - 2\varepsilon$ [35]. No such correlations for predicting incipience of transition in developing/simultaneously developing flows with respect to wall roughness are available. However, as will be discuss shortly, correlations for estimating pressure drop for developing turbulent flow in rectangular channels do indicate the same trend in the change of slope as compared to those correlations which are applicable for developing laminar flows; this, when compared to experimental data, suggests, at the least, a drift away from laminarity at Re ≈ 1100. The same has also been confirmed by predictions from the numerical model.

For fully-developed laminar flow in circular channels, Poiseuille number (Po) remains constant and equals 64. For rectangular cross-section, Po decreases with increase in aspect ratio (α) of the cross-section. For the mini-channel under study (aspect ratio $\alpha \approx 0.7$), Po is found to be 58.4 under fully-developed conditions, as per Eq. (2) [31]

$$\mathrm{Po}_{\mathrm{fd}} = 96\left(1 - 1.3553\alpha + 1.9467\alpha^2 - 1.7012\alpha^3 + 0.9564\alpha^4 - 0.2537\alpha^5\right) \quad (2)$$

The raw pressure-drop data given in the inset of Fig. 5 is converted to Po vs Re and depicted in Fig. 5 (main figure). Using analysis suggested by Kline and McClintock [36] the uncertainty in the estimation of experimental Po is found to be ±7.5% in laminar region with low Reynolds number and decreasing to about ±4.0% in the region showing transitional character. For benchmarking the data, the constant value line of Po = 58.4, representing fully-developed conditions in the channel is also depicted. At very low Re, flow will be fully developed for most part of the channel length and therefore the experimental Po is closer to $\mathrm{Po}_{\mathrm{fd}}$. As the flow Re increases, the flow development length inside the channel increases (as noted on Fig. 4) and the deviation from the fully-developed value of Po is clearly seen. Numerical simulation (using the laminar flow model, as described in Section 4) clearly shows the effect of flow development on Po as Re increases. The experimental data closely follows the numerical predictions till Re ≈ 1100 after which the enhanced slope in the experimental Po is visible. As the flow drifts away from laminarity, the slope of variation of Po with flow Re increases. With the simultaneous superposition of flow development phenomenon in the entire length of the channel after Re ≈ 1100 and incipience of transitional behavior, the observed experimental Po starts increasing faster after Re ≈ 1100; the laminar numerical model then starts under-predicting the Poiseuille number.

Next, the experimental results are compared with the correlations available in the literature for predicting pressure drop for developing flows in circular and rectangular ducts. As noted in the literature review, two common length scales used for analysis are (a) hydraulic diameter (b) square root of the area of cross-section. Both these length scales are explored in the results given hereunder.

For benchmarking the data against circular channels, the correlation given by Shah [37] is taken first, which is applicable for laminar hydrodynamically developing flow in circular channels and is valid for the entire range of x_+

$$\mathrm{Po} = \frac{\Delta P}{\frac{1}{2}\rho u^2 x_+} = \left[13.74\sqrt{x_+} + \frac{1.25 + 64x_+ - 13.74\sqrt{x_+}}{1 + 0.00021(x_+)^{-2}}\right]\frac{1}{x_+} \quad (3)$$

Shah [37] also proposed a closed form equation for laminar hydrodynamically developing flow in rectangular ducts, as follows:

$$\mathrm{Po} = f_{\mathrm{app}}\mathrm{Re} = \frac{13.74}{\sqrt{x_+}} + \frac{4f\cdot\mathrm{Re} + \frac{K(\infty)}{x_+} - \frac{13.74}{\sqrt{x_+}}}{1 + C(x_+)^{-2}} \quad (4)$$

where values of $K(\infty)$, fRe and C are taken from Table 1 for channel aspect ratio of 0.5 and 1.0 (for details please refer Refs. [31,37]). The aspect ratio of channels used in the present experimental study is 0.7; it is expected that estimated Po values for this aspect ratio lie between Po values corresponding to those for aspect ratio 0.5 and 1.0.

Fig. 5 also shows the comparison of Eqs. (3) and (4) with the best linear fit of the experimental data in the laminar region of the flow (100 < Re < 1100). Here the length scale used for calculations is the hydraulic diameter. As expected, Eq. (3) predicts larger pressure drop than Eq. (4) and the experimental data is satisfactorily in line with the latter, with the range of experimental uncertainty.

For comparing the data in the transitional regime (after Re > 1100) the closest available correlation proposed by Phillips [38] is chosen, which is actually applicable for Re > 2300, both for

Table 1
$K(\infty)$, $f\cdot$Re, and C values to be used in Eq. (4).[a]

Aspect ratio (α)	$K(\infty)$	$f\cdot$Re	C
0.5	1.28	15.548	0.00021
1	1.43	14.227	0.00029

[a] No explicit values are given for $\alpha = 0.7$ in Refs. [31,37].

developing and developed turbulent flow region in circular tubes, given as

$$\mathrm{Po} = 4 \cdot A \mathrm{Re}^{(1+B)} \tag{5}$$

where $A = 0.0929 + 1.01612 D_h/x$ and $B = -0.268 - 0.3193 D_h/x$

For rectangular tubes, Phillips [38] suggests to replace the characteristic length in Re by

$$L_c = [(2/3) + (11/24) \cdot \alpha(2-\alpha)] D_h \tag{6}$$

The comparison is again shown on Fig. 5 which comes out to be good both in terms of the slope and the absolute values.

A closer look at the inclination of Po vs Re curve as predicted by the correlations in the laminar and turbulent regions clearly show the change in slope between the two regimes. This is in line with the trend noted in the experimental data also at about Re ≈ 1100, suggesting commencement of a shift away from laminarity.

Next, the use of square root of the cross-sectional flow area as the suitable length scale for rationalizing the experimental data is explored. Muzychka and Yovanovich [17] presented a model for laminar hydrodynamically developing flows in rectangular ducts explicitly in terms of duct length x_+ and aspect ratio α; this correlation is also valid for the entire range of x_+

$$\mathrm{Po} = f_{\mathrm{app}} \cdot \mathrm{Re}_{\sqrt{A}} = \left[\left(\frac{13.74}{\sqrt{x_+}} \right)^2 + \left(32\sqrt{\pi} g(\alpha) \right)^2 \right]^{0.5} \tag{7}$$

where $g(\alpha)$ is a geometrical shape function, which is expressed as follows:

$$g(\alpha) \approx \left[1.086957^{(1-\alpha)} \left(\sqrt{\alpha} - \alpha^{\frac{3}{2}} \right) + \alpha \right]^{-1} \tag{8}$$

The expression of shape function is valid over the range $0.05 \le \alpha \le 1$. Here, $\sqrt{A}$ = square root of flow cross-sectional area, is chosen to be the characteristic length, unlike hydraulic diameter. Therefore, in Eq. (7),

$$x_+ = \frac{x}{\sqrt{A} \cdot \mathrm{Re}_{\sqrt{A}}} \tag{9}$$

and

$$\mathrm{Re}_{\sqrt{A}} = \frac{\rho_f \cdot u \cdot \sqrt{A}}{\mu_f}. \tag{10}$$

For the tested channel, $\sqrt{A} = 0.922$ mm while $D_h = 0.907$ mm. Fig. 6 shows the comparison of the data with Eq. (7) for the laminar zone. As can be seen (i) the change of length scale does not substantially affect the data distribution as compared to earlier choice of hydraulic diameter (ii) the correlation given by Muzychka and Yovanovich [17] somewhat over-predicts the mean experimental data by about 5–11%.

Thus, it is noted that the experimental data for pressure drop is fully predictable by the available correlations for developing flows, within the experimental range of uncertainty. Also, the numerical model predicts the trends very effectively till $Re \approx 1100$ after which laminar flow is seen to drift toward transition.

5.2. Heat transfer

The peripheral average local Nusselt number for the rectangular duct employed in the present study is defined as

$$\mathrm{Nu}_x = h_x \cdot D_h / k_f \tag{11}$$

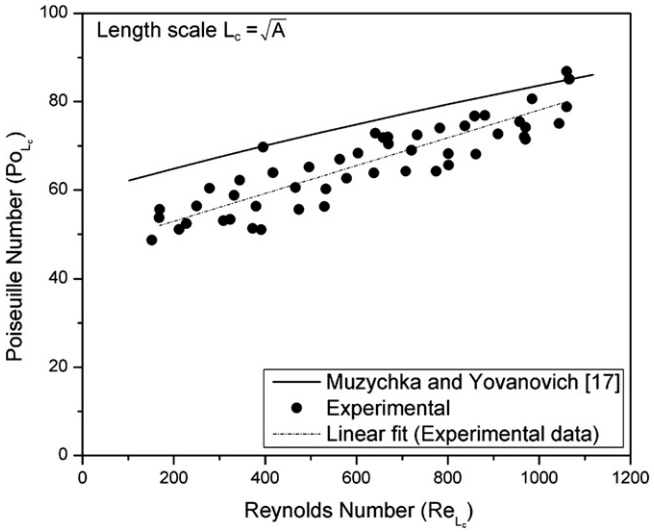

Fig. 6. Po vs Re for the laminar data set plotted using square root of the cross-sectional flow area as the length scale.

where the local heat transfer coefficient is obtained as follows:

$$h_x = \dot{q}'' / \left(T_{w-m} - T_{f-m} \right) \tag{12}$$

For all subsequent data processing, unless otherwise stated, the following two definitions for the wall and fluid temperatures, respectively, are used. Also, the non-dimensional length for the thermal problem is given by $x^+ = x/\mathrm{RePr}D_h$.

- Definition #1: For experimental data reduction,
  T_{w-m} = local wall temperature as measured by the thermocouples T1 and T2 respectively
  T_{f-m} = linearly interpolated value between the fluid inlet and outlet temperatures at channel cross-section corresponding to the two thermocouples locations T1 and T2;

As regards the heat flux $\dot{q}''$ in Eq. (12), experimental data can only be processed by $\bar{\dot{q}}''_{\mathrm{conv}}$, the average heat flux based on applied constant heat power Q at the substrate bottom and the channel heat transfer area $((2\delta_f + w)L)$ from $x = 0$ to $x = L$. The local true wall heat flux $\dot{q}''_{\mathrm{conv}}|_{x^+}$ at a specified location x^+ is not available in the experiment.

- Definition #2: For numerical data reduction,
  T_{w-m} = peripheral averaged wall temperature at location x^+
  T_{f-m} = channel cross-section area averaged fluid temperature at location x^+

For processing the data from the numerical model, both $\bar{\dot{q}}''_{\mathrm{conv}}$ and $\dot{q}''_{\mathrm{conv}}|_{x^+}$ are available and will be used as per the intended discussion. Eq. (11) with Definition #2 and $\dot{q}'' = \dot{q}''_{\mathrm{conv}}|_{x^+}$ gives the 'true' local Nusselt number which uniquely approaches the fully-developed flow value for large x^+.

Before proceeding to discuss the experimental results, the effect of axial conduction during simultaneously developing flow in the test section is explored with the help of the numerical model. We need to consider simultaneous competing effects of convective heat transfer in the channel and conduction heat transfer in the solid array/substrate material. The three natural non-dimensional parameters of this problem are: (i) Number of transfer units of the system, NTU, (ii) Biot number defined on the basis of the thickness of the substrate (see Fig. 1c) and (iii) the wall size ratio, defined as

$$\mathrm{NTU} = \frac{h \cdot L}{\rho_f \cdot c_{p-f} \cdot \delta_f \cdot u}, \quad \mathrm{Bi} = \frac{h \cdot \delta_w}{k_w}, \quad \text{and} \quad \xi = \frac{\delta_w}{L} \tag{13}$$

To physically interpret the results and to highlight the effect of axial conduction in the substrate, Maranzana et al. [39] have combined the above three non-dimensional numbers to define the axial conduction number M, as follows:

$$M = \frac{\dot{q}''_{\mathrm{cond}||}}{\dot{q}''_{\mathrm{conv}}} = \left(k_w \frac{(\delta_w \cdot p)/L}{\left(\rho_f \cdot c_{p-f} \cdot \delta_f \cdot p \cdot u\right)} \right) = \frac{\xi^2 \cdot \mathrm{NTU}}{\mathrm{Bi}} \tag{14}$$

Here, $\dot{q}''_{\mathrm{cond}||}$ gives the first-order estimation of the axial heat flux in the wall, assuming the transfer is one dimensional along the length of the channel through the same temperature difference which the fluid experiences between channel inlet and outlet. The parameter M allows the comparison of the axial heat transfer by back conduction in the substrate wall to the convective heat transfer to the fluid. Naturally, if the value of M is high, axial conduction effects are important and cannot be neglected. In the experimental program, the constant heat flux is applied at a certain distance from the channel walls, as seen in Figs. 1c and 3. Thus, the actual thermal boundary condition experienced by the fluid at the channel walls will deviate from true 'constant heat flux' due to the change in the effective value of parameter M. We note here that for specified duct geometry and a given heat transfer fluid, the parametric variation of $M \cdot (\mathrm{Re} \cdot \mathrm{Pr})$ will highlight the effect of the thermal conductivity of the substrate material (assuming constant thermophysical properties with temperature), as given by

$$M \cdot (\mathrm{Re} \cdot \mathrm{Pr}) = \left(\frac{D_h}{L}\right) \cdot \left(\frac{\delta_w}{\delta_f}\right) \cdot \left(\frac{k_w}{k_f}\right) \tag{15}$$

where

$$\mathrm{Pr} = \left(\frac{c_{p-f} \cdot \mu_f}{k_f}\right) \tag{16}$$

The present experiments on the copper mini-channel array with the specified geometry and water as the working fluid have been performed at $M \cdot (\mathrm{Re} \cdot \mathrm{Pr}) \sim 114$ and 139 respectively. All other conditions remaining the same, if the substrate material was chosen to be of lower thermal conductivity, say $k_w = 16.0$ W/m K (representative value of stainless steel), then the corresponding values of $M \cdot (\mathrm{Re} \cdot \mathrm{Pr})$ would have been equal to ~4.7 and 5.75 respectively.

To highlight the effect of the parameter M on the array under study, the variation of heat flux ratio (actual peripheral averaged heat flux experienced by the fluid at the wall at a given location (i.e. $\dot{q}''_{\mathrm{conv}}|_{x^+}$) to the heat flux averaged over the entire channel area from $x = 0$ to $x = L$, i.e. $\bar{\dot{q}}''_{\mathrm{conv}}$) along the length of Channel #4, as a function of axial heat conduction number M is plotted, as shown in Fig. 7. The cases corresponding to $M = 0.2334$, 0.1535 and 0.0900 have been simulated on the actual experimental array ($k_w = 389$ W/m K) for flow Re = 150, 228, 389 respectively. The cases corresponding to $M = 0.0100$, 0.0066 and 0.0039 have been simulated taking a stainless steel substrate ($k_w = 16$ W/m K), again at flow Re = 150, 228, 389 respectively. For all cases, the fluid inlet temperature as well as the applied heat power on the bottom of the substrate is held constant. It is evident that for the cases where M is high there is considerable back conduction in the substrate from the downstream direction toward the channel inlet, clearly showing conjugate nature of heat transfer. In such cases the actual peripheral averaged wall heat flux on the channel wall near the inlet is considerably higher than in the downstream direction. For a constant heat input to the substrate, the fluid outlet temperature

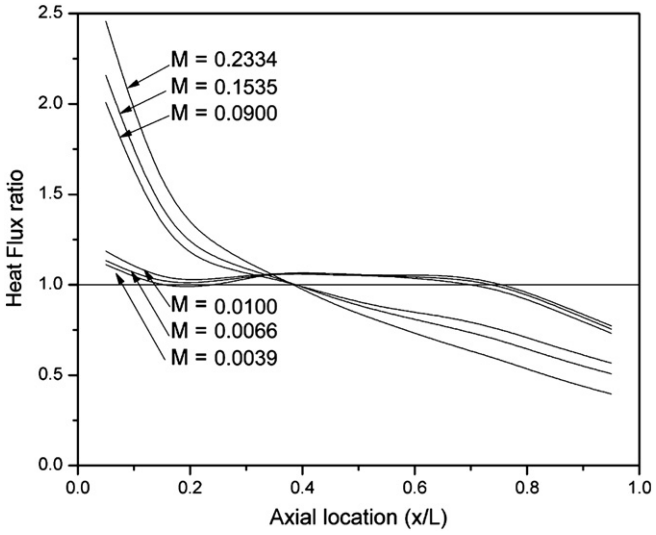

Fig. 7. Variation of heat flux ratio along the length of the channel (Channel number 4).

(as well as the corresponding wall temperature) goes down with increase in flow Re (decrease in M). This decreases the non-uniformity in the actual heat flux experienced by the fluid along the length of the channel. For low values of M, the constant heat flux condition is seen to be approximately maintained throughout the channel length. Typically, when the value of M is of the order of 10^{-2} or lower, conjugate effects are seen to have minimal influence.

The manifestation of this conjugate nature of heat transfer on the variation of the local Nusselt Number (Nu_x) in the channel, with changes in the effective M, is depicted in Fig. 8. Here, Definition #2 has been used, as noted above, for $T_{w\text{-}m}$ and $T_{f\text{-}m}$, along with $\dot{q}''_{\mathrm{conv}}|_{x^+}$, thus giving the true local Nu_x. Cases with a higher value of M lead to decreased estimation of local Nu_x (the mean Nusselt number will correspondingly decrease too). It should be noted that Fig. 8 has been obtained for Pr = 3.25. The variation of Nu_x with x^+ is a function of Pr; as Pr increases the local Nu_x at any given location x^+ will decrease because the flow increasingly becomes more developed at that location.

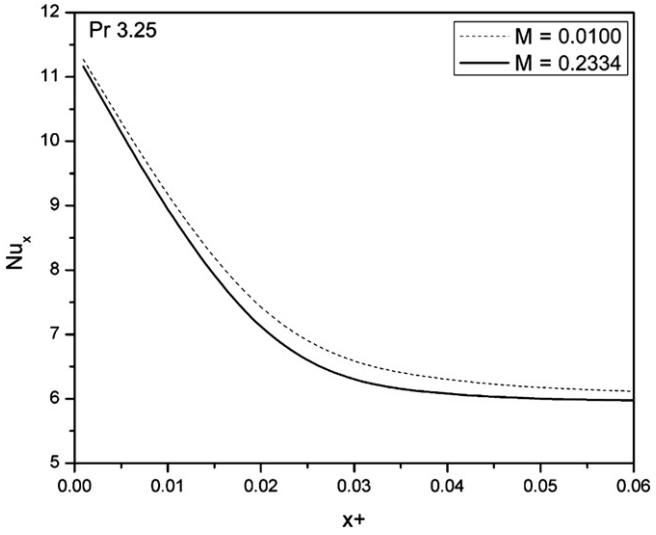

Fig. 8. Variation of the local Nusselt number (Nu_x) along the channel with changes in the axial conduction number M.

Next, the effect of parameter $M\cdot(\mathrm{Re}\cdot\mathrm{Pr})$ on the mean local wall and fluid temperatures along the axial direction in the test array is explored. This is depicted in Fig. 9a–c, which plots $T_{w\text{-}m}$ and $T_{f\text{-}m}$ expressed in non-dimensional form ($T^* = (T - T_i)/(T_o - T_i)$) along the length of Channel #4 of the array as obtained from the simulation. All other conditions remaining the same, the simulation is done for flow Re = 150, 389 and 1815 respectively. The axial location of thermocouples T1 and T2 which measure actual $T_{w\text{-}m}$ along the test section with their respective experimental values are also shown for reference. Many interesting heat transfer features can be deduced from this result. The effect of parameter $M\cdot(\mathrm{Re}\cdot\mathrm{Pr})$ is addressed first on low and high Reynolds number flows.

5.2.1. Case (i)-Low flow Re

At low Reynolds number (Re = 150), the flow quickly develops both hydrodynamically and thermally, inside the channel. There is considerable variation in the $T_{w\text{-}m}$ and $T_{f\text{-}m}$ with the change in $M\cdot(\mathrm{Re}\cdot\mathrm{Pr})$. At low value of $M\cdot(\mathrm{Re}\cdot\mathrm{Pr})$, when the conjugate heat transfer effects are less pronounced (M is less for the specified Re),

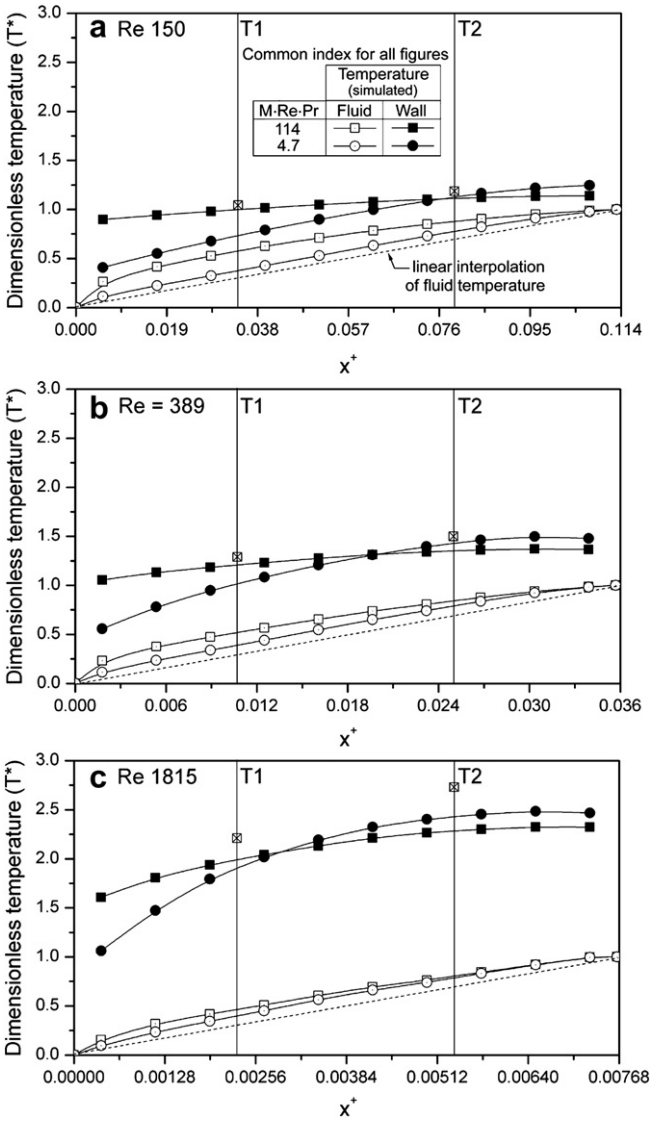

Fig. 9. Effect of parameter $M\cdot(\mathrm{Re}\cdot\mathrm{Pr})$ on the mean local wall and fluid temperatures in the test array.

$T_{w\text{-}m}$ and $T_{f\text{-}m}$ have practically a constant and equal slope and the axial variation of $T_{f\text{-}m}$ comes close to the theoretical linear increase between inlet and outlet (the dotted line represents the linear variation); clear signs of near fully-developed conditions. For this low flow Re though, when $M\cdot(\mathrm{Re}\cdot\mathrm{Pr})$ increases to 114, there is a drastic change of slope, both for $T_{w\text{-}m}$ and $T_{f\text{-}m}$. The wall temperature at the upstream location tends to be much higher as compared to the previous case of lower $M\cdot(\mathrm{Re}\cdot\mathrm{Pr}) = 4.7$. A clear tendency of 'isothermalization' of the wall temperature is seen due to strong conjugate heat transfer. Also, increase in mean $T_{f\text{-}m}$ is quite nonlinear with more increase (higher slope) in the early sections of the channel length than at downstream locations. Moreover, if the local Nu_x at locations corresponding to thermocouples T1 and T2 by the model (essentially adopting Definition #1 and $\dot{q}'' = \bar{\dot{q}}''_{\mathrm{conv}}$) is estimated, then Nu_x at location T1 ($\mathrm{Nu}_{\mathrm{T1}}$) will come out to be lower than Nu_x at location T2 ($\mathrm{Nu}_{\mathrm{T2}}$) viz., the temperature difference $(T_{w\text{-}m} - T_{f\text{-}m})$ is decreasing in the axial direction, $\dot{q}''$ being taken as a constant $= \bar{\dot{q}}''_{\mathrm{conv}}$; this is quite contrary to the expected result for developing flows, wherein Nu_x at the downstream direction should be lower than the upstream direction, as was shown earlier in Fig. 8.

5.2.2. Case (ii)-High flow Re

As flow Re increases to 1815 (here laminar flow is assumed for simulations), the array is subjected to simultaneous flow development across major portion of the channel. In such cases, for equal corresponding values of $M\cdot(\mathrm{Re}\cdot\mathrm{Pr})$, the axial conduction number M comes out to be quite low than at Re = 150 and 389 respectively. The axial variation of $T_{f\text{-}m}$ is now closer to linear, suggesting near constant heat flux experienced by the fluid at the channel walls. In addition, the temperature difference $(T_{w\text{-}m} - T_{f\text{-}m})$ along the downstream direction is very close to the ideal non-conjugate case, i.e. the difference is seen to increase, at least for the case $M\cdot(\mathrm{Re}\cdot\mathrm{Pr}) = 4.7$ because of the fact that discrepancy between $\bar{\dot{q}}''_{\mathrm{conv}}$ and $\dot{q}''_{\mathrm{conv}}|_{x^+}$ is decreasing.

In addition, as can be seen, the effective temperature difference $(T_{w\text{-}m} - T_{f\text{-}m})$ using Definition #1 is considerably larger than by using Definition #2. Therefore, at all axial locations the Nu_x, if calculated from Definition #1 with $\dot{q}'' = \bar{\dot{q}}''_{\mathrm{conv}}$ (either by experiment or by model) will always come out to be smaller than the 'true' local Nu_x based on Definition #2 with $\dot{q}'' = \dot{q}''_{\mathrm{conv}}|_{x^+}$, as is seen next in Fig. 10. The error in the estimation of local Nu_x from the experiment will primarily consist of two-parts (a) error due to the actual location of the temperature sensor from the wall, which will lead to discrepancy in estimating the true wall temperature, and (b) error due to linear interpolating of the mean fluid temperature between the fluid inlet and outlet temperature; this error will decrease with decreasing M, as seen in Fig. 9.

In view of the above discussion, the experimental estimation for local Nu_x in the array is now addressed. Fig. 10a and b depicts the variation of experimental local Nu_x ($T_{w\text{-}m}$ and $T_{f\text{-}m}$ from Definition #1 above with $\dot{q}'' = \bar{\dot{q}}''_{\mathrm{conv}}$) with respect to flow Re, at two thermocouple locations T1 and T2 along the length of the mini-channels, for Pr = 3.25 and 3.97, respectively. For direct one-to-one comparison of the experimental data with the model, the simulation results for local Nu_x, by taking the same Definition #1 of $T_{w\text{-}m}$ (here, the simulated value of temperature at actual location of the thermocouples, i.e. 2.5 mm below the bottom wall of the Channel #1 at $x = 15$ and 35 mm, respectively, have been taken) and $T_{f\text{-}m}$ (linearly interpolated value of fluid temperature between inlet and outlet) with $\dot{q}'' = \bar{\dot{q}}''_{\mathrm{conv}}$, have also been plotted on Fig. 10. The 'true' local Nu_x by taking Definition #2 with $\dot{q}'' = \dot{q}''_{\mathrm{conv}}|_{x^+}$ is also depicted here. Finally, for benchmarking the data with fully-developed flow in rectangular channels with constant heat flux condition at three sides and insulation at fourth side (as in the present experiments);

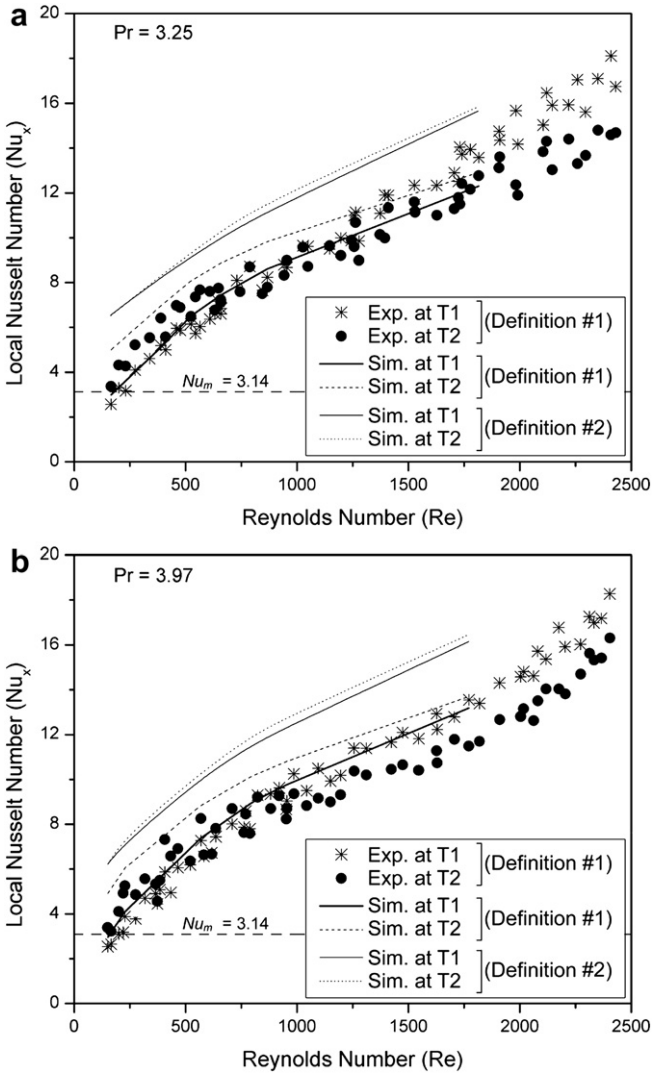

Fig. 10. Variation of local Nusselt number (Nu_x) with flow Re and its comparison with the numerical predictions.

the mean Nusselt number is also plotted on Fig. 10. This is given by [40][2]

$$Nu_m = 8.235\left(1 - 1.883\alpha + 3.767\alpha^2 - 5.814\alpha^3 + 5.361\alpha^4 - 2\alpha^5\right) \tag{17}$$

where, α is the aspect ratio given by: length of insulated side/length of adjacent side. This equation is valid for all cases where the insulated side is smaller than the adjacent side so that α is always less than one. For $\alpha > 1$, the above equation is not valid; for such cases, Shah and London [31] provide tabular as well as graphical data which can be approximated within ±1.5% by the following equation:

$$Nu_m = 5.202\left(1 - 3.087\beta + 9.822\beta^2 - 16.335\beta^3 + 13.823\beta^4 - 4.554\beta^5\right) \tag{18}$$

[2] This equation is explicitly mentioned in Ref. [40]; it can also be obtained by curve fitting of the graphical data given in Shah and London [31].

where, β = length of adjacent side/length of insulated side; here again $0 \le \beta \le 1$. For the present case $\beta = 0.7$ and Nu_m from Eq. (18) comes out to be 3.14.

The following salient features can be noted from this figure:

(i) The experimental data clearly show that at low flow Re, local Nu_{T1} is indeed smaller than Nu_{T2}. The data thus provides quite a misleading picture of developing flows at low Re, unless seen in the context of conjugate effects and axial heat transfer, as discussed earlier with reference to Figs. 7 and 9. As the flow Re increases, thereby decreasing the value of parameter M, the experimental data clearly indicate dilution of the conjugate effects; local experimental Nu_{T1} becomes comparable to Nu_{T2}, eventually becoming larger than it for Re > 1100. This reveals that negligence in *a priori* estimation of axial heat conduction number M may lead to erroneous conclusions about local heat transfer coefficients.

(ii) The one-to-one comparison of local Nu_x from experiment and simulation, employing the same definition of $T_{w\text{-}m}$ and $T_{f\text{-}m}$, i.e. from Definition #1 above, with $\dot{q}'' = \bar{\dot{q}}''_{conv}$, matches quite satisfactorily suggesting soundness of the numerical model in predicting the experimental data in a manner it is processed. For the entire range of flow Re, simulated local Nu_{T1} is also smaller than Nu_{T2}. The reasons for this behavior have been explained earlier in the context of Fig. 9. As the flow Re increases (M decreases), the difference between simulated Nu_{T1} and Nu_{T2} is seen to progressively decrease, indicating reduced effects of axial back conduction. As noted earlier in Fig. 9, numerical calculations have been done up to Re = 1815 using the laminar model. After Re > 1100, while the experimental data suggests that $Nu_{T1} > Nu_{T2}$ as expected under minimal or no conjugate effects, the laminar numerical model after Re > 1100 does not capture this experimental trend. This again suggests that the flow is drifting away from laminarity in the experiment; incipience of turbulence in the experiment increases the heat transfer and further reduces the effects due to conjugate heat transfer; this is not captured by the laminar simulation model after Re > 1100.

(iii) The 'true' local Nu_x by taking Definition #2 with $\dot{q}'' = \dot{q}''_{conv}|_{x^+}$ is indeed higher than the experimentally estimated local Nu_x, the latter being calculated using Definition #1 with $\dot{q}'' = \bar{\dot{q}}''_{conv}$. The discrepancy is of the order of 50% at very low flow Re which reduces to about 25% as Re increases. The reasons for this have also been delineated earlier in the context of Fig. 9. In addition, at very low flow Re, since the flow development length is very small, true Nu_x at location T1 and T2 are nearly the same. Thus, due to strong conjugate effects, especially at low Re (high M) under developing flow conditions, estimations from experimental data may not only lead to erroneous conclusions, but also the absolute values of transport coefficients will be considerably underestimated.

6. Summary and conclusions

Simultaneously developing flows provide very high heat transfer coefficients in the entrance regions and therefore of interest for mini/microscale high heat flux removal applications. In this work such flows have been experimentally and numerically investigated through a mini-channel array. The array consisted of fifteen rectangular parallel channels ($w = 1.1 \pm 0.02$ mm, $\delta_f = 0.772 \pm 0.005$ mm, and $D_h = 0.907$ mm), machined on a copper plate of 8 mm thick. Flow Re was varied from 150 to 2500 while inlet flow Pr was maintained in the range of 3–4. The main conclusions of the study are:

(i) The experimental setup was scrutinized for equivalence of flow distribution across all the channels with the help of the numerical model. The design of the inlet plenum for fluid entry provided sufficiently good flow distribution; the maximum discrepancy was less than 3.4%.

(ii) The experimental and theoretical Po, as well as Nu_x, is a function of flow Re. The data suggests an early incipience of transition from laminarity, i.e. near Re ≈ 1100. This is primarily deduced from the trends of the raw experimental data, comparison of the experimental data with well established correlations and predictions obtained from numerical modeling. The difference between the experimental pressure drop and laminar numerical model starts increasing after Re ≈ 1100. Similar trend is obtained in the heat transfer data too. Apart from the fact that transition occurs early, no new physical phenomena or effects are observed in the data.

(iii) The square root of cross-section area of the fluid flow was also explored as a possible length for scaling; no significant improvement was observed by this choice of the length scale, in the range of the experimental conditions.

(iv) Numerical investigation of the exactness of the constant heat flux boundary condition at the channel wall was done with the help of the heat conduction number (parameter M). The study clearly reveals that due to axial back conduction in the substrate, conjugate effects become predominant at higher values of parameter M. It was demonstrated that the experimental data, especially at low flow Re, is therefore affected, leading to lower estimations of local Nusselt numbers. The variation of local Nusselt number along the axial direction also gets affected due to the parameter M. It is emphasized that *a priori* knowledge of the axial conduction number is vital for achieving correct data reduction during experiments. All other parameters remaining identical, substrates with low thermal conductivity reduce effects of axial conduction, under constant heat flux boundary condition.

Most parallel channels connected to a common inlet header will have fully or partially developing flows; such designs appear frequently in engineering and other domains. Depending on the substrate geometry and flow conditions (i.e. parameter M), conjugate heat transfer effects may become predominant in such systems; therefore, the data should be carefully interpreted in this context for generating correct design estimates.

Acknowledgments

The work is funded by the Department of Science and Technology, Government of India, under the sponsored project No: DST/CHE/20060304 titled 'Micro-devices for Process Applications'.

References

[1] S.G. Kandlikar, W.J. Grande, Evolution of microchannel flow passages – thermohydraulic performance and fabrication technology, Heat Transf. Eng. 24 (2003) 3–17.
[2] K.V. Sharp, R.J. Adrian, J.G. Santiago, J.I. Moiho, Liquid flows in microchannels. in: M. Gad-el-Hak (Ed.), The MEMS Handbook. CRC Press, Florida, USA, 2001 [Chap. 6(I)].
[3] D.B. Tuckerman, R.F. Pease, High performance heat sinking for VLSI, IEEE Electr. Dev. Lett. 2 (1981) 126–129.
[4] P.Y. Wu, W.A. Little, Measurement of friction factor for the flow of gases in very fine channels used for micro miniature Joule-Thompson refrigerators, Cryogenics 23 (1983) 273–277.
[5] A.B. Duncan, G.P. Peterson, Review of microscale heat transfer, Appl. Mech. Rev. 47 (1994) 397–428.
[6] S.S. Mehendale, A.M. Jacobi, R.K. Shah, Fluid flow and heat transfer at micro- and meso-scales with application to heat exchanger design, Appl. Mech. Rev. 53 (2007) 175–193.
[7] B. Palm, Heat transfer in microchannels, Microscale Thermophys. Eng. 5 (2001) 155–175.
[8] C.B. Sobhan, S.V. Garimella, A comparative analysis of studies on heat transfer and fluid flow in microchannels, Microscale Thermophys. Eng. 5 (2001) 293–311.
[9] N.T. Obot, Towards a better understanding of friction and heat/mass transfer in microchannels – a literature review, Microscale Thermophys. Eng. 6 (2002) 155–173.
[10] S.V. Garimella, C.B. Sobhan, Transport in microchannels – a critical review, Annu. Rev. Heat Transf. 13 (2003) 1–50.
[11] G.P. Celata, M. Cumo, G. Zummo, Thermo-hydraulic characteristics of single-phase flow in capillary pipes, Exp. Thermal Fluid Sci. 28 (2004) 87–95.
[12] G.L. Morini, Single-phase convective heat transfer in microchannels: a review of experimental results, Int. J. Thermal Sci. 43 (2004) 631–651.
[13] S.G. Kandlikar, S. Garimella, D. Li, S. Colin, M. King, Heat Transfer and Fluid Flow in Minichannels and Microchannels. Elsevier, London, 2006.
[14] P.S. Lee, S.V. Garimella, Thermally developing flow and heat transfer in rectangular microchannels of different aspect ratios, Int. J. Heat Mass Transf. 49 (2006) 3060–3067.
[15] P.S. Lee, S.V. Garimella, D. Liu, Investigation of heat transfer in rectangular microchannels, Int. J. Heat Mass Transf. 48 (2005) 1688–1704.
[16] M. Bahrami, M.M. Yovanovich, J.R. Culham, Pressure drop of fully developed laminar flow in microchannels of arbitrary cross-section, J. Fluids Eng. 128 (2006) 1036–1044.
[17] Y.S. Muzychka, M.M. Yovanovich, Modeling friction factors in non-circular ducts for developing laminar flow, in: Proc. 2nd AIAA Theoretical Fluid Mechanics Meeting, Albuquerque, USA, 1998.
[18] G.P. Celata, M. Cumo, V. Marconi, S.J. McPhail, G. Zummo, Microtube liquid single-phase heat transfer in laminar flow, Int. J. Heat Mass Transf. 49 (2006) 3538–3546.
[19] M.E. Steinke, S.G. Kandlikar, J.H. Magerlein, E.G. Colgan, A.D. Raisanen, Development of an experimental facility for investigating single-phase liquid flow in microchannels, Heat Transf. Eng. 27 (2006) 41–52.
[20] L. Zhigang, G. Ning, M. Takei, An experimental investigation of single-phase heat transfer in 0.045 mm to 0.141 mm microtubes, Nanoscale Microscale Thermophys. Eng. 11 (2007) 333–349.
[21] C.Y. Yang, T.Y. Lin, Heat transfer characteristics of water flow in microtubes, Exp. Thermal Fluid Sci. 32 (2007) 432–439.
[22] H.S. Park, J. Punch, Friction factor and heat transfer in multiple microchannels with uniform flow distribution, Int. J. Heat Mass Transf. 51 (2008) 4535–4543.
[23] N. García-Hernando, A. Acosta-Iborra, U. Ruiz-Rivas, M. Izquierdo, Experimental investigation of fluid flow and heat transfer in a single-phase liquid flow micro-heat exchanger, Int. J. Heat Mass Transf. 52 (2009) 5433–5446.
[24] V.K. Natarajan, K.T. Christensen, The impact of surface roughness on flow through a rectangular microchannel from the laminar to turbulent regimes, Microfluidics Nanofluidics 9 (2010) 95–121.
[25] Z. Liu, C. Zhang, X. Zhao, Experimental study on influence of microscale effects on liquid flow characteristic in micro-tubes, Heat Mass Transf. 45 (2009) 297–304.
[26] M. Rao, S. Khandekar, Simultaneously developing flows under conjugated conditions in a mini-channel array: liquid crystal thermography and computational simulations, Heat Transf. Eng. 30 (2009) 751–761.
[27] Z.H. Guo, Z.X. Li, Size effect on single-phase channel flow and heat transfer, Int. J. Heat Fluid Flow 24 (2003) 284–298.
[28] H. Herwig, O. Hausner, Critical view on 'New results in micro-fluid mechanics': an example, Int. J. Heat Mass Transf. 46 (2003) 935–937.
[29] J.R. Kinglsey-Rowe, G.D. Lock, J.M. Owen, Transient heat transfer measurements using thermochromic liquid crystal: lateral-conduction error, Int. J. Heat Fluid Flow 26 (2005) 256–263.
[30] W.M. Kays, M.E. Crawford, Convective Heat and Mass Transfer. McGraw Hill Inc., New York, 1993.
[31] R.K. Shah, A.L. London, Laminar Flow Forced Convection in Ducts. Academic Press, New York, 1978.
[32] X. Wang, X.F. Peng, Experimental investigation of liquid forced-convection heat transfer through micro-channel, Int. J. Heat Mass Transf. 37 (1994) 73–82.
[33] M.E. Steinke, S.G. Kandlikar, Single-phase liquid friction factors in microchannels, Int. J. Thermal Sci. 45 (2006) 1073–1083.
[34] S.G. Kandlikar, S. Joshi, S. Tian, Effect of surface roughness on heat transfer and fluid flow characteristics at low reynolds numbers in small diameter tubes, Heat Transf. Eng. 24 (2003) 4–16.
[35] S.G. Kandlikar, D. Schmitt, A.L. Carrano, J.B. Taylor, Characterization of surface roughness effects on pressure drop in single-phase flow in minichannels, Phys. Fluids 17 (100606) (2005) 1–11.
[36] S.J. Kline, F.A. McClintock, Describing uncertainties in single-sample experiments, Mech. Eng. 75 (1953) 3–6.
[37] R.K. Shah, A correlation for laminar hydrodynamic entry length solutions for circular and noncircular ducts, J. Fluids Eng. 100 (1978) 177–179.
[38] R.J. Phillips, Microchannel heat sinks, Ph.D. Thesis, Massachusetts Institute of Technology, USA, 1987.
[39] G. Maranzana, I. Perry, D. Maillet, Mini- and micro-channels: influence of axial conduction in the walls, Int. J. Heat Mass Transf. 47 (2004) 3993–4004.
[40] L.P. Yarin, A. Mosyak, G. Hetsroni, Fluid Flow, Heat Transfer and Boiling in Micro-Channels Series: Heat and Mass Transfer. Springer, 2009, ISBN 978-3-540-78754-9.